Auger decay of excitons in Cu_2O

K. E. O'Hara, J. R. Gullingsrud, and J. P. Wolfe
Physics Department and Materials Research Laboratory, University of Illinois at Urbana-Champaign, Urbana, Illinois 61801
(Received 1 February 1999)

The nonradiative recombination of an exciton due to a collision with another exciton (i.e., Auger recombination) is the dominant loss mechanism for excitons at high densities in photoexcited Cu_2O. The principal evidence is that (a) the observed lifetime of excitons shortens substantially at high densities, and (b) the exciton density increases sublinearly with increasing excitation power. To achieve exciton densities at which this two-body decay process comes into play, the particles are produced within a few micrometers of the crystal surface using intense pulsed excitation with photon energies well above the semiconductor band gap. In the past, determination of the ''Auger constant'' A in the two-body decay rate, $1/\tau = An$, was limited by insufficient knowledge of the exciton density n. In the present work, we have determined the density of excitons by (a) measuring their absolute brightness in a calibrated optical system and (b) measuring the expanding volume occupied by the excitons. The luminescence signal following subnanosecond laser excitation exhibits a decay rate which is strongly dependent on the particle density. While some modeling is required to determine the volumes at earliest times, we believe that we have determined the Auger constant to within a factor of 2. The experimental value, $A = 7 \times 10^{-17}$ cm^3/ns, is nearly two orders of magnitude larger than that derived from spectroscopic analysis. Such a strong Auger decay prevents the gas from achieving average densities in the quantum statistical regime of an ideal gas. [S0163-1829(99)13239-9]

I. INTRODUCTION—EXCITONS IN Cu_2O

Cuprous oxide (Cu_2O) provided the first convincing evidence of excitons in a semiconductor crystal. The fact that an electron and a hole can bind into a positroniumlike species—the exciton—was demonstrated through optical absorption measurements showing a classic Rydberg series of excited states. Early measurements concentrated on the spectroscopic properties of the exciton. The measured binding energy of the exciton is 150 meV, corresponding to a Bohr radius of only about 7 Å.

Photoluminescence experiments show that there are orthoexcitons (angular momentum triplet) and paraexcitons (angular momentum singlet) composed of spin-1/2 electrons and holes. Due to the parity-forbidden energy gap in Cu_2O, the direct orthoexciton transition is only quadrupole allowed. The paraexciton lies 12 meV lower than the orthoexciton due to exchange interaction, and its direct transition is forbidden to high order. Phonon-assisted transitions reveal the kinetic-energy distributions of both species. The phonon-assisted radiative rate is 500 times larger for orthoexcitons than for paraexcitons.

Excitons act as free particles with a center-of-mass momentum and kinetic energy; this has been previously demonstrated in several types of photoluminescence experiments. For lattice temperatures above about 30 K, the luminescence spectra show kinetic-energy distributions of particles obeying Maxwell-Boltzmann statistics at or near the lattice temperature. Also, photoluminescence *imaging* experiments directly measure the macroscopic diffusion and drift of excitons under a variety of conditions.

In the present paper we are concerned with a density-dependent nonradiative decay process that tends to limit the exciton density, as is apparent in Fig. 1. We use 10-ns pulses of 514.5-nm light from a cavity-dumped argon-ion laser, which has a 3-μm absorption length in Cu_2O,[1] to produce a dense gas of electron-hole pairs. The left-hand inset of Fig. 1 indicates the excitation geometry. The sample is in a 2-K liquid helium bath. A 50-μm diameter aperture is lightly pressed on the sample and a laser beam illuminates this region uniformly. The electron-hole pairs form excitons, and the Γ_{12}^- phonon-assisted orthoexciton luminescence, shown in the right-hand inset, is proportional to the total number of orthoexcitons in the crystal. The time-integrated luminescence (circles) increases sublinearly as the power is increased, showing that a density-dependent recombination

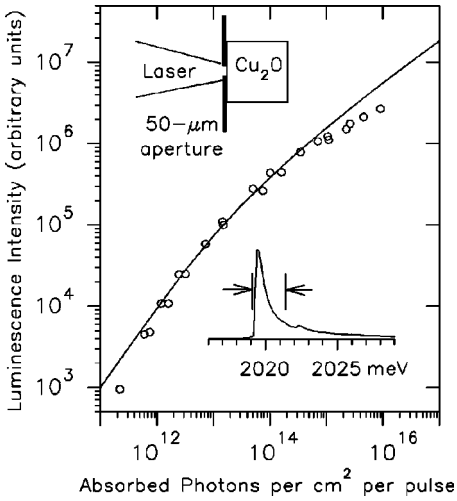

FIG. 1. Time-integrated orthoexciton luminescence resulting from a range of intensities of pulsed argon-ion laser excitation. The curve is the prediction of a model assuming Auger recombination with the rate determined in this article, scaled to the data. Left inset: excitation geometry. Right inset: time-integrated spectrum, for 10^{15} photons per cm^2, showing the range of spectral integration used.

mechanism begins to limit the exciton density at moderate excitation levels.

In semiconductors where electrons and holes remain unbound in a plasma, one can observe a process in which an electron recombines with a hole and transfers its band-gap energy to another nearby electron or hole. This three-body process is called Auger recombination. In Cu_2O at low temperatures, the excitons are the dominant species, and the density-dependent decay is due to the collision of two excitons. One exciton recombines and the other is split into a free electron and hole that carry away the band-gap energy. Following Hulin *et al.*,[2] we refer to this two-*exciton* decay process as Auger recombination.

The instantaneous decay rate of excitons due to this two-body decay process is $1/\tau_A = An$, where A is the Auger constant. For steady-state excitation, this process leads to a sublinear dependence of exciton density on incident power. Returning to Fig. 1, the solid curve is the predicted time-integrated luminescence intensity assuming Auger recombination of the magnitude determined in this article.

Because of its effectiveness in limiting exciton density, and in continuously producing high-energy electron-hole pairs, Auger decay has become central to understanding the behavior of the excitonic gas at high densities, especially in the quest for Bose-Einstein condensation of excitons.

II. RELATION TO QUANTUM STATISTICS

Typical photoluminescence experiments on this system employ optical excitation with energies much larger than the band gap, so the electronic excitations must cool towards the lattice temperature by emitting phonons. An important consequence of this short-wavelength excitation is that the optical absorption length is just a few micrometers, thus the excitons are initially formed within a small volume. This is an obvious advantage if one wants to study the excitonic gas at high densities.

Figures 2 and 3 show the results of such intense optical excitation. In Fig. 2 a 250-ps argon-ion laser pulse excites a crystal of mineral Cu_2O immersed in a bath of liquid nitrogen at 70 K.[3] Photoluminescence spectra from orthoexcitons are recorded with a time resolution of 400 ps and are fit reasonably well by Maxwell-Boltzmann energy distributions.[4] Figure 2(b) shows the effective temperature of the gas determined by these fits. The kinetic-energy relaxation due to acoustic phonon emission has been studied extensively.[5]

The experimental spectra undergo a striking transformation as the lattice temperature is lowered. Figure 3(a) shows time-resolved spectra under the same conditions as in Fig. 2, but with a helium bath temperature of 2 K. The spectra are now well described by a Bose-Einstein distribution, as studied extensively by our research group[6,7] and first reported by Hulin *et al.*[2] In those previous studies, the densities of excitons were obtained by a fit to the Bose-Einstein distribution,

$$n(\varepsilon) = \frac{g(\varepsilon)}{e^{(\varepsilon-\mu)/kT}-1}, \tag{1}$$

where $g(\varepsilon)$ is the density of states for excitons with kinetic energy ε. The shape of the spectrum determines T and μ, and the density follows as the integral of $n(\varepsilon)$.

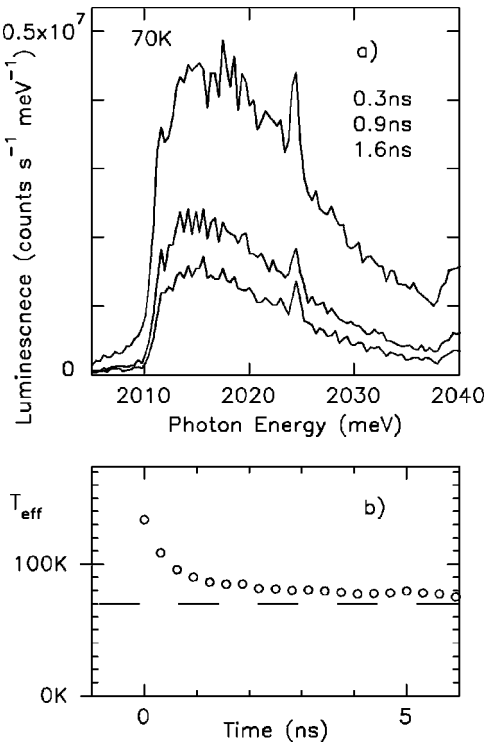

FIG. 2. (a) Successive orthoexciton luminescence spectra from a 70-K crystal after a 10-nJ argon-ion laser pulse with FWHM of 250 ps. These spectra are well fit by a Maxwell-Boltzmann distribution with temperature T_{eff}. (b) Apparent gas temperature as a function of time. The apparent decay time of approximately 400 ps is limited by the temporal resolution of the photomultiplier tube. The dashed line shows the bath temperature.

The resulting plot of n_{fit} *vs* T, given in Fig. 3(b), is similar to the results reported earlier by Snoke, Wolfe, and Mysyrowicz,[6] and shows a ''quantum saturation'' near the predicted phase boundary for Bose-Einstein condensation. Experiments by Goto *et al.*[8] and Naka *et al.*[9] find similar orthoexciton spectra. Furthermore, evidence of a condensed component has been reported by Lin and Wolfe[7] for paraexcitons and by Shen *et al.*[10] for orthoexcitons.

Such spectra occur only with high-intensity excitation. At low excitation density, the gas quickly cools to the lattice temperature.[11] The gas temperature falls more slowly at high excitation levels. A key issue is why the gas is warmer at high densities. Of course, the gas is most dense at early times when it is still cooling. It was first postulated by Mysyrowicz *et al.*[12] that the Auger process acts to heat the gas at high densities. Simply stated, the hot electrons and holes created by Auger decay possess initial kinetic energies approaching 1 eV; as they cool, these hot carriers scatter with the remaining excitons, thereby heating the gas. This process has been studied theoretically by Kavoulakis, Baym, and Wolfe.[13] Its importance is obvious in Fig. 3(b): Auger heating is apparently preventing the quantum gas from crossing the phase boundary for Bose-Einstein condensation.

Taken together, the data of Figs. 2 and 3 raise serious questions about the existence of quantum statistics in these experiments. Both the 70-K and 2-K data are produced by the same excitation conditions. Consider the spectra at a sampling time of 300 ps. The total luminescence intensities obtained by integrating over each spectrum are found to be

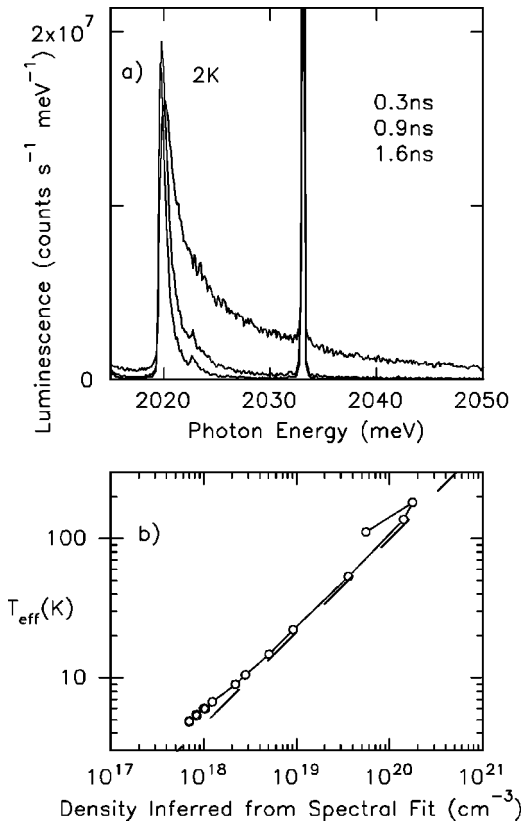

FIG. 3. (a) Successive orthoexciton luminescence spectra from a 2-K crystal, with all other experimental conditions the same as in Fig. 2. The broad peak is phonon-assisted luminescence; the narrow peak is direct luminescence. Note the change in vertical scale between Figs. 2 and 3 and the spectral shift due to the band-gap shift. (b) Apparent gas temperature vs the gas density inferred from the spectral shape using Eq. (1), and allowing for instrumental resolution and Lorentzian broadening of the spectrum. This curve is parameterized by time, with the dots marking 312 ps intervals. The maximum temperature coincides with the laser pulse at 0 ps. The dashed line shows the critical density for Bose-Einstein condensation for an ideal gas.

almost identical at this early sampling time ($I_{70K}=0.78I_{2K}$). Also, the fitted temperatures of the gases are considerably higher than the lattice temperatures and are quite similar in magnitude (e.g., 100 K vs 140 K at $t=300$ ps). If the same number of excitons at the same *gas temperature* are occupying the same volume, we expect them to exhibit the same statistics. Yet the ''70-K'' spectrum is a classical distribution, and the ''2-K'' spectrum is apparently in the quantum regime!

What are the gas volumes? Unfortunately, they are difficult to measure directly; however, previous work showed that the diffusivity of paraexcitons decreases with increasing lattice temperature due to more frequent exciton-phonon scattering. Thus, it is reasonable to assume that the gas volume at a lattice temperature of 70 K will be less than that at 2 K. For our experiment, this would cause a higher degeneracy in the ''70-K'' spectrum than in the ''2-K'' spectrum, contrary to the observations. We conclude from these experiments that neither experiment has an average gas density sufficient to reach the quantum statistical regime.

What, then, is the origin of the quantumlike distributions? One might postulate that at low lattice temperatures the gas undergoes a spatial condensation into high-density droplets, similar to the condensation of excitons into electron-hole droplets in Ge and Si. In those cases, however, the condensed phase had a unique spectral luminescence that was shifted from the exciton line due to the liquid binding energy. In the present case, the low-energy edge of the orthoexciton spectrum is virtually unshifted as the density level is increased into the ''quantum regime.'' In other words, there appears to be no binding energy to cause a spatial condensation. In a later paper we will study the possibility that the sharply peaked distributions are due to a combination of many processes: phonon emission, diffusion, and Auger recombination.

Snoke, Wolfe, and Mysyrowicz[6] were cautious about relying on spectroscopic data to determine the exciton densities: they performed time-resolved imaging experiments to estimate the gas volume. Assuming that each photon in the excitation pulse produced one exciton, they concluded that the average density within the measured volumes was in reasonable agreement with the spectroscopically determined densities. Their estimate, however, did not allow for significant losses due to Auger recombination.

Several attempts have been made to measure the important Auger constant A. The first mention and characterization of this process was by Mysyrowicz *et al.*,[12] who recognized its role in limiting the exciton densities. Unfortunately, their estimate, $A=2\times10^{-19}$ cm^3/ns, did not allow for the reduction in exciton density by diffusion, since their experiment predated the first report[14] of the unusually high diffusivity of paraexcitons in Cu_2O. Using 100-ps pulses and time-resolved luminescence, Snoke and Wolfe[11] observed a density-dependent decay rate that led to a value of $A=10^{-18}$ cm^3/ns. However, they assumed densities from the quantum statistical analysis of luminescence spectra, which are now subject to question. In a quite different set of experiments, Trauernicht, Wolfe, and Mysyrowicz[15] determined a value of $A=7\times10^{-17}$ cm^3/ns for paraexcitons confined to a parabolic strain well.[16]

Our present studies attempt to experimentally measure the elusive Auger constant for orthoexcitons. Our systematic approach is as follows: (1) calibration of our optical system in order to measure the total number of excitons from their brightness, (2) determination of the production efficiency of the short-wavelength excitation by comparison with resonant volume excitation, and (3) measurement of the gas volume by luminescence imaging with sufficient time and space resolution. We begin with a theoretical description of the transient behavior of an excitonic gas undergoing Auger recombination and report several new experiments that demonstrate the general features of this process.

III. PROPERTIES OF THE AUGER RECOMBINATION PROCESS

For a gas of orthoexcitons of density n in a cold lattice, a simplified description of their decay is given by a single rate equation,

$$\frac{dn}{dt}=-\frac{n}{\tau}-An^2+G, \tag{2}$$

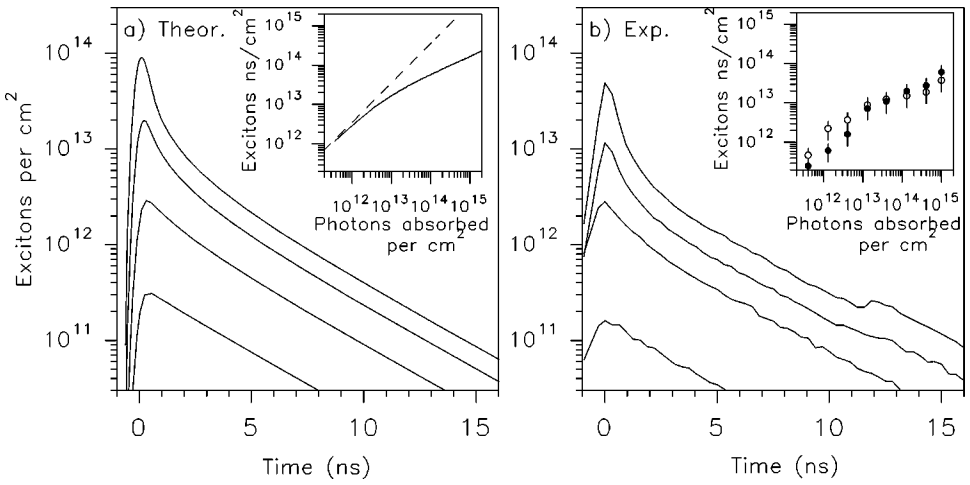

FIG. 4. (a) Results of numerically integrating Eq. (2) for a source $G(r,t)$ which is Gaussian in time, and exponential in space, modeling the creation of excitons using light with an absorption length $d=3.0$ μm. The four curves correspond to 1.3×10^{12},1.3×10^{13},1.3×10^{14}, and 1.3×10^{15} photons absorbed per cm^2. This model assumes a 30% production efficiency, $\tau=3.5$ ns and $A=7\times10^{-17}$ cm^3/ns. Inset: the integral over time and depth into the crystal of $n(r,t)$ vs the integral of $G(r,t)$. (b) Areal density of orthoexcitons determined by photoluminescence resulting from 0.5-ns argon-ion laser pulses using the geometry of Fig. 1. Absorbed power was 1.3×10^{12},1.3×10^{13},1.3×10^{14} and 1.0×10^{15} photons absorbed per cm^2. Inset: time-integral of the observed density of orthoexcitons (dots) and paraexcitons (circles).

where τ is the single-particle lifetime, A is the Auger constant, and G is the generation rate in units of orthoexcitons per unit volume per unit time.

We use the Auger constant A, rather than a cross section, because the Auger recombination rate can reasonably be expected to remain finite as the exciton momentum goes to zero.[17] Suppose the matrix element for Auger recombination is nonzero for two excitons at rest. In contrast to the case of elastic scattering, the density of final states for the ejected electron and hole depends little on the initial exciton momenta. Fermi's golden rule would yield a finite recombination rate for a gas of excitons at rest. We are also ignoring the dependence of A on the exciton relative wave vector k. Because the Bohr radius of an exciton is 0.7 nm, we would expect a k dependence of A on the scale of $k\sim1.4$ nm^{-1}. An exciton with this k has energy 25 meV, greater than the energy of most of the excitons in our experiments. We attempt to measure only the low-k limit of A.

The lifetime τ is most likely controlled by the down-conversion of orthoexcitons to paraexcitons, which is phonon assisted and depends on both the gas and lattice temperatures. At early times, the gas temperature is changing, so τ could vary. We believe, however, that the loss of excitons is dominated by the Auger term at early times. We base this belief on the observation that there is no large increase in the paraexciton luminescence at early times, as would be the case if orthoexciton down-conversion were the dominant nonlinear process.

Assuming that τ is constant, assuming a uniform homogeneous gas, and neglecting the effects of particle diffusion, the transient solution to Eq. (2) with $G=0$ is

$$n(t)=\frac{n_0e^{-t/\tau}}{1+An_0\tau-An_0\tau e^{-t/\tau}}. \tag{3}$$

In practice, however, there is a time-dependent generation rate $G(t)$ corresponding to the optical excitation pulse. In anticipation of the experimental results to follow, we assume a Gaussian pulse with a full width at half maximum (FWHM) of 0.5 ns. The density $n(t)$ is then calculated by numerically integrating Eq. (2). In the calculation, τ is taken to be the measured orthoexciton lifetime at low density, 3.5 ns, and we use $A=7\times10^{-17}$ cm^3/ns obtained from a later analysis in this paper (Sec. V).

When the excitons are generated by light with absorption length d, the generation rate G also depends on the depth into the crystal. This can be taken into account by integrating Eq. (2) with G appropriate for each of several depths, and summing the results. Results of this simulation are shown in Fig. 4 for four pulse powers. The lowest power produces the bottom trace, which displays a single-exponential decay of 3.5 ns, as predicted for $An_0\tau\ll1$ in Eq. (3). The next trace up is obtained for an order-of-magnitude increase in pulse power. The overall signal increases by about an order of magnitude, but the early behavior indicates the onset of the nonexponential Auger decay. Increasing the power by another order of magnitude (the third trace), we see a pronounced effect of Auger decay at early times and the signal at late times is not increased by an order of magnitude, due to the Auger losses at early times. The top trace continues this trend for an additional order-of-magnitude increase in excitation power.

The inset in Fig. 4(a) plots the time-integrated density obtained as the excitation power is increased by over four orders of magnitude. The dependence is linear at low powers and approaches a square-root dependence at high powers. This behavior is a result of the Auger rate An^2 dominating the n/τ rate. The density effectively reaches a steady-state value during the excitation pulse.[18] By setting $dn/dt=0$ in Eq. (2) and ignoring the first term on the right-hand side, we predict a density during the pulse of

$$n=\sqrt{G/A}, \tag{4}$$

explaining the square-root dependence of the peak density on generation rate.

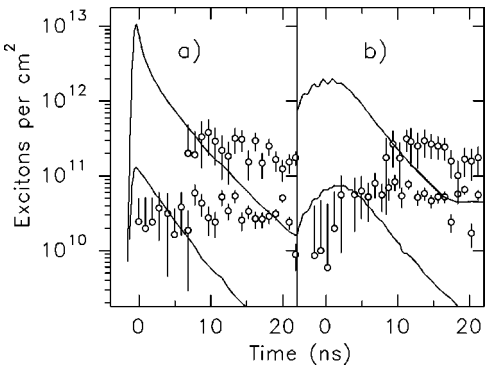

FIG. 5. (a) Areal densities of orthoexcitons (lines) and paraexcitons (circles) following 0.5-ns argon-ion laser pulses depositing 9×10^{11} (lower data) and 9×10^{13} (upper data) photons per cm^2 in the crystal. (Error bars that would extend to the bottom of the plot were omitted for clarity.) (b) The same experiment using 10-ns laser pulses depositing 9×10^{11} and 9×10^{13} photons per cm^2 in the crystal.

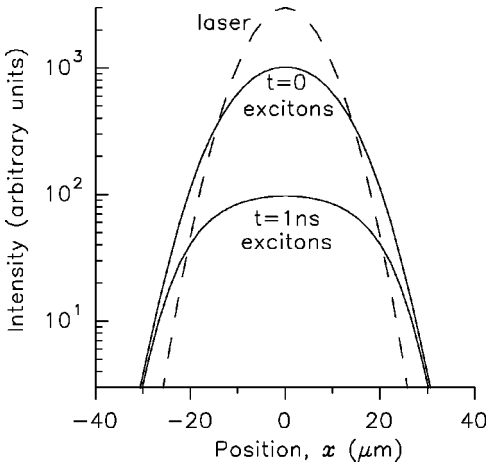

FIG. 6. Result of integrating Eq. (2) using a source with shape $G(r,t)\propto\exp(-(x^2+y^2)/2\sigma^2)\exp(-z/d)\exp(-t^2/2\tau^2)$, where σ represents the Gaussian width of the laser spot (dashed line), d is the 3-μm laser penetration depth, and τ=FWHM/2.35 with FWHM =0.5 ns the width of the laser pulse. The solid lines are predicted luminescence intensity at $t=0$ and $t=1$ ns. In this simulation, the spatial FWHM of the luminescence intensity has increased by a factor of 1.5 during the rapid Auger decay before 1 ns.

Experimental data corresponding to these calculations are shown in Fig. 4(b). These are the spectrally integrated time traces of the phonon-assisted luminescence of orthoexcitons in a mineral crystal at a temperature of 2.0 K. An argon-ion laser beam ($\lambda=514$ nm) with a 0.5-ns pulse width fills a 50-μm diameter aperture on the crystal (Fig. 1, inset). The vertical scale in the figure has been converted to exciton density by using the optical-system calibration described in the next section of this paper.

The data clearly show both the density-independent exponential decay at low densities and the more rapid decay of excitons at high densities, in remarkably good agreement with the simulation in Fig. 4(a). In the inset of Fig. 4(b), we plot the power dependencies of the time-integrated intensities for both orthoexcitions and paraexcitons. Both species display the sublinear increase in density expected for Auger recombination at high excitation density.

So far we have ignored the paraexcitons. Due to their slow radiative rate, and the proximity of the paraexciton luminescence to a brighter orthoexciton phonon replica, we are unable to measure the number of paraexcitons at early times. We *can* observe the number of paraexcitons *after* the laser pulse. Figure 5 shows the relative numbers of orthoexcitons and paraexcitons following laser pulses of two different strengths. The paraexciton number, like the orthoexciton number, increases sublinearly with laser power [see also Fig. 4(b) inset]. We conclude that paraexcitons do suffer Auger decay, but it is not immediately clear whether there are Auger decay events between pairs of paraexcitons, or if ortho-para Auger decay alone limits the paraexciton density.

From our experiments, it is difficult to determine separately the Auger constant for each possible combination of angular momentum states of the colliding excitons. We confine ourselves to considering the effect the paraexcitons may have on our attempt to measure the ortho-ortho Auger recombination rate. We assume that the electron-hole pairs formed by the laser pulse (and those generated by Auger recombination) form excitons with random angular momentum states, i.e., three orthoexcitons for each paraexciton. If the Auger cross-section is independent of the angular momentum states of the colliding excitons, Auger decay will tend to keep the ortho-to-para ratio approximately 3:1, so by ignoring paraexcitons entirely, we would overestimate A by 25%. If, on the other hand, para-para Auger decay is disallowed, but ortho-para Auger decay has the same strength as ortho-ortho Auger decay, the ortho-to-para ratio becomes 2:1; we overestimate A by 33%.[19] We will continue to ignore the paraexcitons, and extract A from our experiments as if ortho-para Auger were forbidden. Future experimental or theoretical work on the dependence of Auger decay on the spin states of the excitons may make it possible to correct the resulting overestimation of A.

Finally, in this section we consider how the Auger process

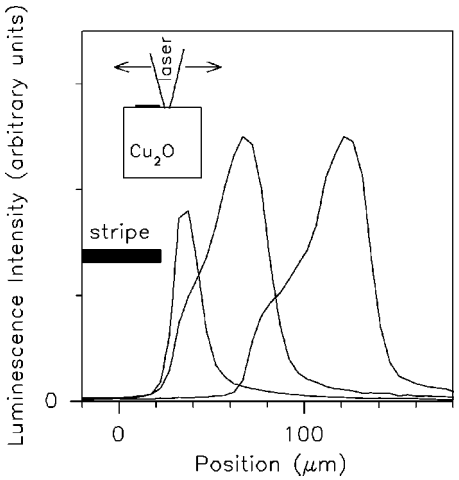

FIG. 7. Spatial profiles orthoexciton luminescence observed during a 200-ps argon-ion laser pulse. The profile at right is considerably broader than the 25-μm full-width of the laser focus. The laser focus was moved toward an opaque metal stripe on the crystal surface, indicated by the dark bar. The center and left profiles correspond to increasing obstruction of the laser beam. The lack of signal under the stripe shows that diffusion is not the cause of the extra width of the exciton cloud.

can affect the spatial distribution of excitons when no aperture is used to define the absorption region—i.e., the usual experimental situation. If the Auger decay process is dominant and the decay rate is shorter than the pulse length, a Gaussian excitation spot, $G \propto \exp(-x^2/2\sigma^2)$, will produce a broader distribution of excitons, $n \propto \exp(-x^2/4\sigma^2)$, due to the square-root dependence in Eq. (4). A simulation of this effect is shown in Fig. 6. In addition, reflections at optical elements and cryostat windows can degrade the laser beam and cause significant non-Gaussian ''wings'' in the excitation profile. These wings become especially prominent when an Auger process is dominant, because the density in the center of the beam is limited more than that in the wings.

In an imaging experiment, it is important to distinguish this ''Auger broadening'' of the excitation volume from the effects of excitonic diffusion. Figure 7 shows spatial profiles of the orthoexciton luminescence as the laser beam is moved closer to a knife edge on the excitation surface, beyond which no excitation occurs. The broad, oddly shaped profiles are not due to excitonic diffusion at these relatively early sampling times. We know this because no signals are observed beyond the knife edge. Instead, the wings in the excitation profile, combined with the nonlinear Auger decay, have produced a broader distribution than that of the excitation profile. In Sec. V we show that this effect leads to an apparent rapid expansion of the exciton gas at early times when the Auger process affects the spatial distribution of excitons.

Consequently, in the presence of Auger recombination, the size of the initial exciton cloud is not simply related to the size of the laser spot. Therefore, as part our measurement of the Auger constant, we must measure the spatial distribution of the excitons directly. In the next section we consider the luminescence rates of excitons and describe how we calibrate our optical system to measure the absolute number of excitons within the field of view.

IV. LUMINESCENCE RATES AND GENERATION EFFICIENCY

As mentioned earlier, the radiative rate $1/\tau_{\rm rad}$ of excitons in Cu_2O is very slow due to the dipole-forbidden direct gap. The actual lifetime τ of the excitons is much shorter than $\tau_{\rm rad}$ due to nonradiative processes. For the orthoexcitons, the limiting decay time of about 3.5 ns at low density in a high-purity sample is most likely due to ortho-to-para conversion. For the paraexcitons, lifetimes up to 13 μs have been observed in mineral crystals.[20] We shall see that even this lifetime is much shorter than the radiative decay time and is probably determined by nonradiative recombination at impurities.

Nevertheless, it is the radiative rate $1/\tau_{\rm rad}$ that determines the brightness of the exciton luminescence. The total rate of photon emission from N excitons is given by $N/\tau_{\rm rad}$. While it is virtually impossible to directly determine the radiative lifetime in a forbidden-gap semiconductor, radiative decay is intimately linked with the inverse process, optical absorption of the exciton band, which can be measured directly.

Figure 8 shows an optical absorption measurement on one of our mineral samples. There is a narrow absorption line at the energy of an orthoexciton. For light traveling along a

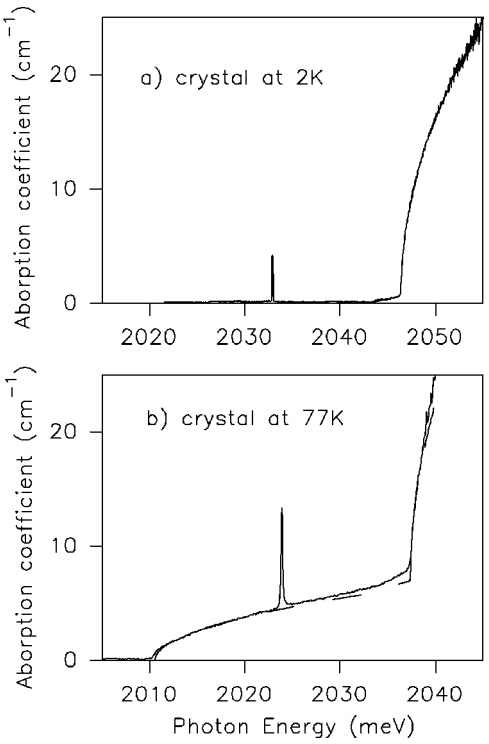

FIG. 8. The sharp absorption line is due to resonant creation of orthoexcitons. At 2 K a strong absorption band due to creation of an exciton and a Γ_{12}^- phonon is observed. If this absorption band is multiplied by f and $(1+f)$, where f is the thermal occupation at 77 K of the Γ_{12}^- phonon, it fits the Stokes and anti-Stokes absorption bands at 77 K (dashed lines) with no adjustable parameters. The crystal used was 2.1 mm thick.

$\langle 100 \rangle$ direction, the integral of this direct absorption line is 1.8 cm^{-1} meV at 77 K, but only 0.6 cm^{-1} meV at 2 K. Kreingol'd and Makarov[21] explain that the absorbance at low temperatures is determined not by the exciton-photon coupling, but by how fast exciton-polaritons are scattered out of the polariton states.

To the right of the direct absorption line, higher by the 13.6-meV energy of a Γ_{12}^- optical phonon, is the onset of a phonon-assisted absorption band, caused by the optical creation of an orthoexciton and an optical phonon. The dipole-allowed absorption coefficient is proportional to the square root of the exciton kinetic energy $\varepsilon = \hbar\omega - \hbar\omega_{\rm onset}$, and is given by

$$\alpha(\varepsilon) = (8.0 \pm 1.0)\,{\rm cm}^{-1}\sqrt{\varepsilon/{\rm meV}}, \tag{5}$$

where the coefficient is our measured value. Equation (5) is superimposed on the data of Fig. 8(a), but is obscured by the data. The 77-K data in Fig. 8(b) shows a similar band with threshold energy 13.6 meV below the direct absorption line. This band corresponds to the annihilation of a thermally excited Γ_{12}^- phonon as the orthoexciton is created. The dashed line is derived from Eq. (5) taking into account the thermal occupation number of Γ_{12}^- phonons at 77 K, as explained in the caption.

We mention a couple of practical details: Using a 10-μm slice of mineral Cu_2O, the absorption length for photons at the wavelength of the 514.5-nm argon-ion laser line is found to be (3.0 ± 0.5) μm, in agreement with previous

measurements.[1] The index of refraction in this region is also of interest. Karlsson *et al.*[22] report that the index of refraction of Cu_2O increases from near 2.6 in the infrared to a peak of 3.1 at 500 nm. In the region of exciton luminescence, around 600 nm, the index of refraction is 3.0.

The relationship between the absorption coefficient and the radiative decay rate is derived using a detailed-balance argument. For each photon, the probability of absorption per unit time is given by $(c/n)\alpha(\varepsilon)$, where c is the speed of light and n is the index of refraction. We consider a crystal in equilibrium with thermal radiation. The rate of photon absorption per unit volume is thus given by[23]

$$\frac{c}{n}\alpha(\varepsilon)\rho(\hbar\omega)f_p(1+f_x),$$

where f_p and f_x are the equilibrium photon and exciton occupation numbers and $\rho(\hbar\omega)=n^3\omega^2/\pi^2c^3\hbar$ is the photon density of states. The rate of luminescence of thermal excitons is

$$\frac{1}{\tau_{\rm rad}}g(\varepsilon)f_x(1+f_p),$$

where $g(\varepsilon)$ is the exciton density of states.

In thermal equilibrium the absorbance and luminescence rates must be equal. Also, because both the photons and excitons involved are bosons with total energy $\hbar\omega$, we have $f_x=f_p=1/(\exp(\hbar\omega/kT)-1)$, implying that

$$\frac{1}{\tau_{\rm rad}}=\frac{c}{n}\frac{\alpha(\varepsilon)\rho(\hbar\omega)}{g(\varepsilon)}=\frac{n^2\omega^2}{\pi^2c^2\hbar}\frac{\alpha(\varepsilon)}{g(\varepsilon)}. \tag{6}$$

The density of states for a free exciton of mass m and band degeneracy g_0 is

$$g(\varepsilon)=\frac{g_0}{4\pi^2}\left(\frac{2m}{\hbar^2}\right)^{3/2}\sqrt{\varepsilon}. \tag{7}$$

For orthoexcitons in Cu_2O, with $g_0=3$ and $m=3m_0$,[24] Eqs. (5–7) yield,

$$\frac{1}{\tau_{\rm rad}}=(7.0\pm1.3)\times10^4/{\rm s}, \tag{8}$$

or $\tau_{\rm rad}=14\ \mu$s, for the Γ_{12}^- phonon-assisted orthoexciton luminescence. Although we considered excitons in thermal equilibrium with their environment, the radiative rate $1/\tau_{\rm rad}$ is a property of the exciton itself. The detailed balance argument is merely the simplest way to relate the two manifestations of the exciton-photon interaction: absorbance and the radiative rate.

We can apply the same relation to the paraexcitons. Paraexcitons interact with light only with the assistance of a Γ_{25}^- optical phonon, and this paraexciton absorption band is 1500 times weaker than the Γ_{12}^- phonon-assisted orthoexciton band.[25] Using this smaller α, the appropriate degeneracy $(g_0=1)$, and the same mass as for the orthoexcitons, we conclude that the radiative lifetime for paraexcitons is approximately $500\times14\ \mu{\rm s}=7$ ms.

To check these predictions, we must (a) calibrate our optical system to measure the number of luminescence photons emitted from a specified volume in the sample, and (b) create a known number of excitons in a well defined observation volume. Salient details concerning the overall collection efficiency of our optical system are as follows (for more detail, see the Appendix). Our $f/2.5$ lens collects a 0.014-steradian cone inside the material $(n=3)$, and we measure a total reflective loss of 53% from various optical surfaces. The combined efficiency of the optical spectrometer, photomultiplier tube, and discriminator is 3.0%. Considering all these factors, we expect each orthoexciton to contribute

$$70000/{\rm s}\times\frac{0.014}{4\pi}\times47\%\times3.0\%=1.1\pm0.3{\rm counts/s}$$

to the count rate, integrated over the Γ_{12}^- phonon-assisted spectral line.

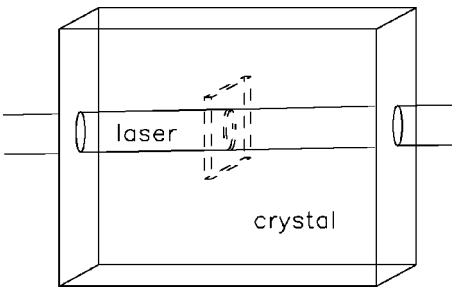

FIG. 9. Experimental geometry used to test our predictions of the exciton luminescence rate and spectrometer efficiency. The dashed box shows the region of crystal from which luminescence is accepted by the monochromator entrance slit.

Figure 9 illustrates how we produce a known number of excitons in a well defined volume. The exciton density must be kept low in order to avoid Auger recombination and maximize the lifetime of the particles. To achieve these conditions, a 10-ns dye-laser pulse with a long absorption length in Cu_2O is used to excite an extended volume in the crystal. The laser is tuned to a photon energy of 2047 meV($\lambda=605.5$ nm) just above the phonon-assisted absorption band [Fig. 8(a)] so as to produce orthoexcitons with very little kinetic energy at the rate of one orthoexciton per photon absorbed. We confirm the absorption length $\alpha^{-1}=1.4$ mm by measuring the intensity of the transmitted laser beam as a function of wavelength.

The number of photons absorbed per centimeter per second is given by $\alpha I(x,t)=\alpha I_0(t)e^{-\alpha x}$, where $I_0(t)$ is the incident photon flux determined from the incident power. For optical excitation in the phonon-assisted absorption band, each photon absorbed creates one orthoexciton, so we know how many excitons are created per second per meter. We collect the orthoexciton luminescence emitted from a small region at position x_0 of width Δx, which corresponds to an image of the entrance slit of our spectrometer on the sample. The total number of excitons created per second in this region is $\alpha\Delta xI_0(t)e^{-\alpha x_0}$.

The solid curve in Fig. 10(a) shows the cumulative number of orthoexcitons produced in the observation region, i.e., $\alpha\Delta xe^{-\alpha x_0}\int_{-\infty}^{t}I_0(t')dt'$. During the 10-ns pulse in the experiment, 2×10^7 orthoexcitons are created in this region. The expected luminescence count rate from 2×10^7 orthoexcitons is $(2\times10^7)(1.1\ {\rm counts/s})=2.2\times10^7{\rm counts/s}$. We have used this correspondence to set the right-hand scale in

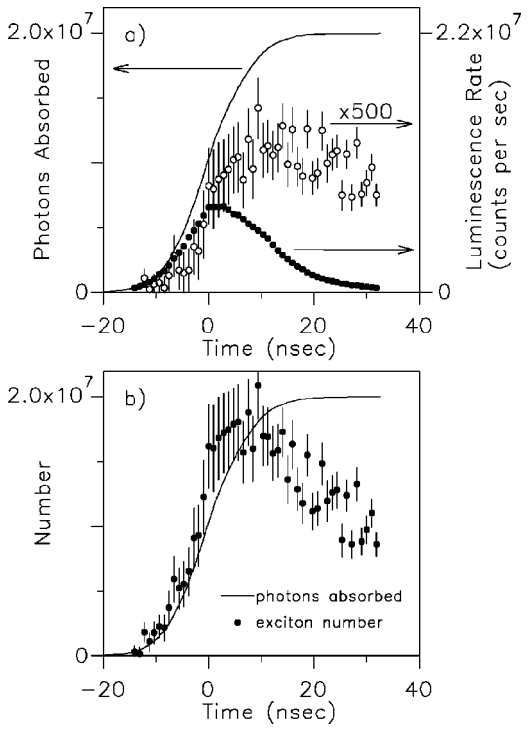

FIG. 10. (a) Line: Cumulative number of dye-laser photons absorbed within the observation region. Dots: time-resolved orthoexciton luminescence. Circles: paraexciton luminescence scaled by its relative radiative efficiency. The two vertical scales have different units; the similarity in their ranges is purely coincidental. Collection efficiency is difficult to control, and varies by as much as a factor of two between experiments. (b) Total number of excitons observed as a function of time, compared to the cumulative number of photons absorbed within the observation region.

Fig. 10. The measured spectrally-integrated count rates from orthoexcitons (dots) and paraexcitons (circles) in this region are shown in the figure.

Figure 10(b) shows the total number of excitons (ortho and para) as determined from their luminescence intensity. The slow decay in exciton number (~20 ns) at later times is due to an unidentified loss mechanism (perhaps exciton trapping) at these low densities. The close correspondence, during the pulse, between the cumulative number of absorbed photons and the sum of the two exciton species confirms our calibration.

Excitation with shorter-wavelength laser light greatly reduces the excitation volume and can affect the efficiency of exciton generation. With 514-nm argon-ion laser light, the 2.4-eV photons produce electron-hole pairs with about 100 meV excess kinetic energy. Losses may occur in the formation of excitons or due to nonradiative decay at the surface. For this reason, we have performed experiments to measure the *exciton production efficiency* for surface excitation, i.e., the thermalized orthoexciton number per laser photon. The excitation geometry is the same as that shown in the inset of Fig. 1. A 50-μm aperture is attached to the excitation surface in order to provide a well defined region of uniform excitation. Luminescence is collected through the surface of the sample opposite the aperture.

Figure 11 shows the results of these experiments. We compare the luminescence produced by 10-ns laser pulses at

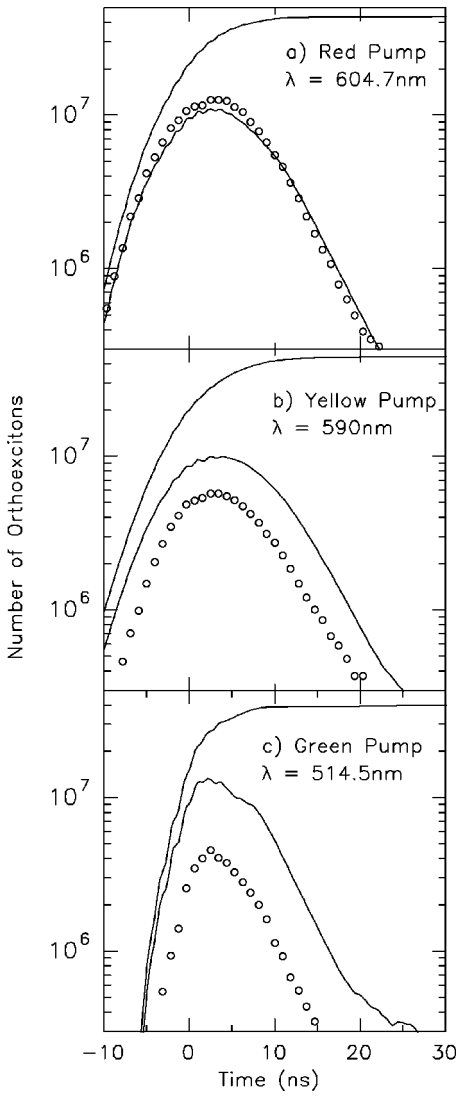

FIG. 11. Production of orthoexcitons by photons of different wavelengths. This experiment used the geometry shown in Fig. 1. Upper curves show the cumulative number of photons absorbed, lower curves include a 3.5-ns decay time for the orthoexcitons. Circles denote the instantaneous number of orthoexcitons determined from the observed luminescence intensity. In each case the lower curves will pass through the data if multiplied by 110%, 50%, and 30%, respectively.

three different wavelengths. The excitation level is low in all cases, less than 10^{16} photons absorbed per cm^3. The entrance slit is widened to accept all the luminescence, and the time-resolved spectra are integrated and converted, using the calibration described above, to a number of excitons. The data in Fig. 11(a), obtained for red light ($\lambda = 604.7$ nm), is similar to that in Fig. 10(a) since the light resonantly creates orthoexcitons in both cases. The absorption length in this case is 1.5 mm, so we expect that surface effects will be negligible and, indeed, the orthoexciton signal is close to that expected if each photon creates one orthoexciton and the orthoexcitons have a 3.5-ns decay time. We conclude that for this volume excitation at 604.7 nm the production efficiency is effectively 100%.

As the laser wavelength is increased to 590 nm in the yellow range, the absorption length decreases to 50 μm,

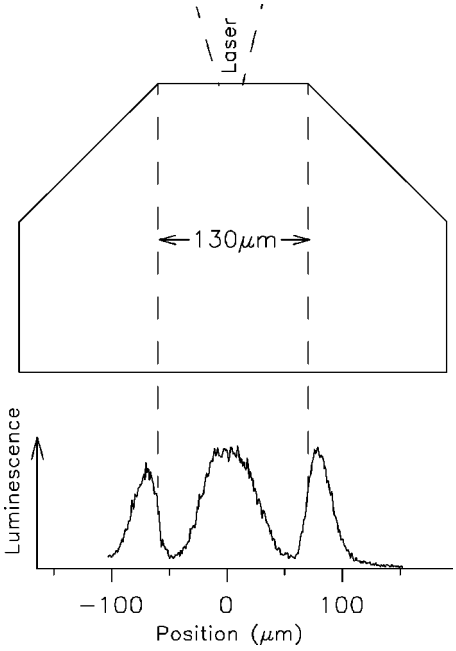

FIG. 12. Experimental geometry (not to scale) for Sec. V. Total internal reflection from the crystal faces at 45° provides spatial profiles of the luminescence, shown at the bottom of the figure, which are orthogonal projections of the orthoexciton density. The data is taken for $t=7$ ns.

and the production efficiency decreases to approximately 50%, as shown in Fig. 11(b). Finally, we arrive at the argon-ion laser excitation, which produces the luminescence signals shown in Fig. 11(c). These data imply a 30% production efficiency of orthoexcitons with argon-ion excitation.

V. DETERMINATION OF THE AUGER CONSTANT

The effective volume of the excitonic gas produced by short wavelengths is difficult to measure directly. As previously indicated, the absorption length in Cu_2O for the 514-nm argon-ion laser is about 3 μm. The highest densities are obtained by focusing the laser beam to its diffraction limit, without the use of an aperture, so the lateral variation in excitation density must be taken into account. To observe the spatial variation of luminescence intensity both laterally and into the crystal, we have devised the crystal shape shown in Fig. 12. As usual, the exciton cloud is viewed through the crystal by scanning an image of the crystal across the entrance slit of the spectrometer. The crystal surfaces that were cut and polished at 45° reflect the luminescence light by total internal reflection, providing the view at right angles to the excitation surface (the ''side view''). An example of the luminescence intensity is shown in the figure. Only orthoexciton luminescence was studied in these high-resolution experiments (the paraexciton signal was too weak).

For these experiments we use a mode-locked cavity-dumped argon-ion laser with a pulse width of 0.5 ns. The pulse repetition rate is 400 kHz and the time-averaged incident power is 4 mW. The laser is focused to a full width at half maximum of $\leqslant 10$ μm. High-resolution scanning of the luminescence image is attained by rotating a quartz block that is placed in front of the spectrometer slit. With the imaging lens set at $f/8$, the spatial resolution of the imaging

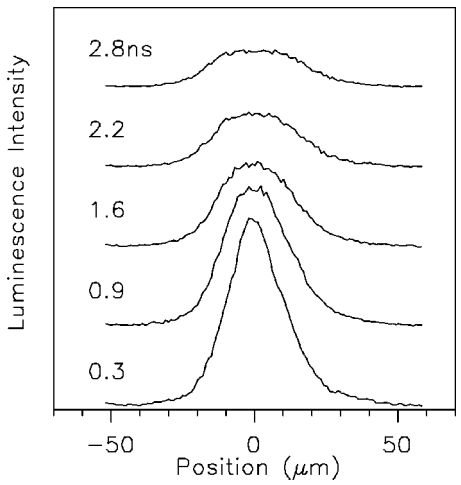

FIG. 13. Spatial profiles of orthoexciton luminescence at several times after a 0.5-ns argon-ion laser pulse containing 10 nJ and focused to 7 μm FWHM.

system is determined to be 6 μm by imaging the weak scattering of luminescence light from the corner where the 45° surfaces meet. This high resolution is obtained with a narrow entrance slit of the spectrometer (20 μm, corresponding to 4 μm on the sample). The spatial scans are taken with a wide exit slit, corresponding to a spectral range of 2.4 meV. The time-resolved photon-counting system has a measured time resolution of 400 ps.

Spatial scans of the orthoexciton luminescence are plotted in Fig. 13. These close-up scans show the exciton cloud expanding from a FWHM of about 13 μm to about 34 μm between 0 and 2.5 ns. The broader scan in Fig. 12 indicates the luminescence profile at 7 ns, under the same experimental conditions. The side-view profiles at the earliest times were obstructed by slight rounding of the crystal surfaces at the corners, but this later profile shows that the expansion distance into the crystal is approximately equal to the lateral expansion distance.

For a diffusion process, we expect the spatial profiles to have the form $n(r,t)=n_0\exp(-r^2/4Dt)$, where D is the dif-

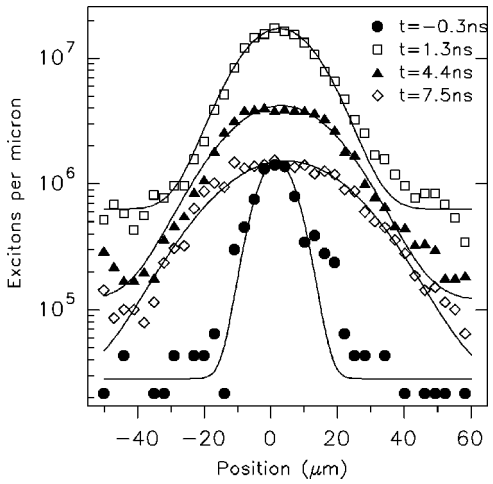

FIG. 14. Semilogarithmic plot of the same data set as Fig. 13, converted to exciton density and fit to Gaussians. Note that the relative intensities are preserved in this plot.

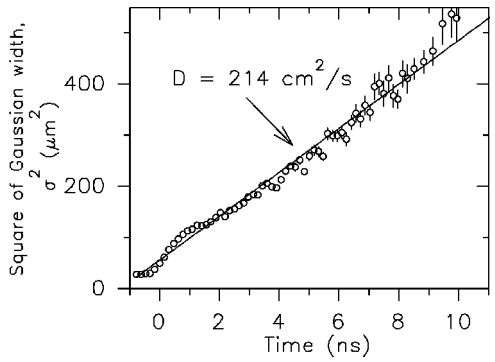

FIG. 15. Square of the Gaussian width of the exciton cloud vs time. The expansion is fit by a diffusivity of 214 cm^2/s (solid line).

fusion constant and $4Dt=2\sigma^2$ for a Gaussian distribution. The width of the distribution, therefore, is given by $\sigma=\sqrt{2Dt}$. Figure 14 shows fits of the lateral-expansion data to Gaussian profiles. Note that the scale is logarithmic and that all the signals are plotted with the same gain, and a small baseline (probably accounting for scattered light) was added to each Gaussian function. The Gaussian profiles give a reasonable approximation to the data, and the a plot of σ^2 vs time is given in Fig. 15. At the later times, the data fit well to a straight line, giving the diffusion constant $D=$slope/2 $=214$ cm^2/s.

This value of D is somewhat smaller than the value of 600 cm^2/s measured by Trauernicht and Wolfe[14] for *paraexcitons* over a much longer time scale. The difference can be reasonably explained by the fact that orthoexcitons scatter both LA and TA phonons, while paraexcitons scatter LA phonons only.

Extrapolating the straight line back to $t=0$ in Fig. 15, we obtain a residual width $\sigma_0^2=(6.4\ \mu m)^2$, corresponding to a FWHM $\equiv 2.355\sigma=15$ μm. Accounting for the spatial resolution of 6 μm, this analysis says that the extrapolated initial cloud width is approximately 14 μm. The measured FWHM of the cloud distribution at the earliest times is actually 12 ± 3 μm, in good agreement. According to our earlier analysis (Fig. 6), if the excitons are in the strong Auger regime at the earliest times, a Gaussian laser spot with a FWHM of 8 μm would give rise to a cloud of this dimension.

Assuming an optical absorption length of 3 μm for the excitation light, Auger broadening would produce an initial half width at half maximum (HWHM) of 4 μm. Thus the cloud is not far from hemispherical initially (the lateral HWHM is 6 ± 1 μm), and the data at late times in Fig. 12 shows virtually the same HWHM for front and side views of the cloud. We therefore assume that for times later than 0.5 ns, the cloud volume is proportional to σ^3, using the measured lateral σ. This function is plotted on a logarithmic scale in Fig. 16.

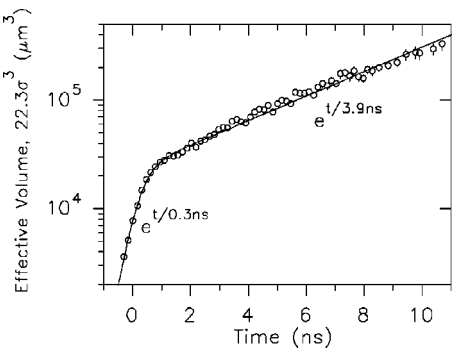

FIG. 16. Effective volume, as defined by Eq. (11), of the exciton cloud vs time. The fit is the sum of two exponentials, given by Eq. (13). The fast exponential rise is probably limited by our timing resolution.

The data reveal two regimes: during the first 0.5 ns a rapid apparent expansion occurs, followed by the normal diffusion at later times. Over the range of observation, these regimes can be empirically represented by exponential functions with time constants of 0.3 and 3.9 ns. The rapid rise in σ^3 at early times may be associated with the Auger broadening effect described earlier, or could represent enhanced particle transport during the hot initial stages of the gas. Note, however, that the initial time constant (0.3 ns) is approximately equal to the time resolution of the photon-counting system, so the physical processes are actually more rapid than this measured value.

At each point in the inhomogeneous particle distribution, Eq. (2), the differential equation describing two-body decay, holds. To relate this model to experimentally measured quantities, we integrate over space. For an exciton density $n(r,t)$, the total number of excitons is $N(t)=\int n(r,t)d^3r$, where the integral extends over the half space beginning with the crystal surface. Letting I denote the corresponding spatial integral of the generation rate G, Eq. (2) yields

$$\frac{dN(t)}{dt}=-\frac{N(t)}{\tau}-A\int n^2(r,t)d^3r+\int G(t)d^3r \quad (9a)$$

$$=-\frac{N(t)}{\tau}-A\frac{N(t)^2}{V(t)}+I(t), \quad (9b)$$

where the last equation defines an *effective volume* of the gas

$$V(t)=\frac{\left(\int n(r,t)d^3r\right)^2}{\int n^2(r,t)d^3r}. \quad (10)$$

For a Gaussian distribution of particles,

$$n(r,t)=\frac{2N(t)}{(2\pi\sigma^2)^{3/2}}e^{-r^2/2\sigma^2},$$

integrating over the half space we find,

$$V(t)=22.27\sigma^3. \quad (11)$$

This effective volume must be used to determine the Auger constant A.

The solution to the differential equation, Eq. (9), including this volume function may now be written [assuming constant τ and $I(t)$ a δ function at time t_0]

$$N(t)=\frac{N_0e^{-(t-t_0)/\tau}}{1+AN_0\int_{t_0}^{t}e^{-(t'-t_0)/\tau}/V(t')dt'}. \quad (12)$$

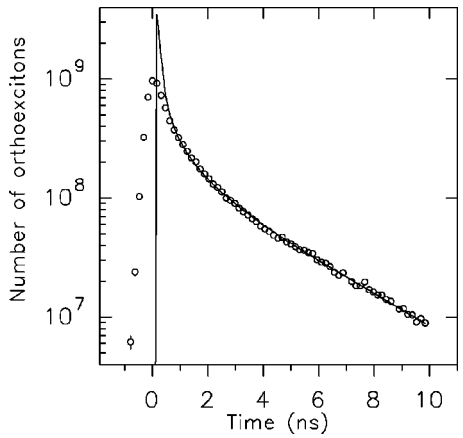

FIG. 17. Number of orthoexcitons, determined from luminescence intensity, vs time after a 10-nJ laser pulse. The fit is Eq. (12) with $A=6.6\times10^{-17}\mathrm{cm}^3/\mathrm{ns}$.

The integration could be performed analytically if $1/V(t)$ were a sum of exponentials. This is a good approximation, as seen in Fig. 16, where the empirical curve is

$$\frac{1}{V(t)}=\frac{\exp(-t/0.30\ \mathrm{ns})}{12000\ \mu\mathrm{m}^3}+\frac{\exp(-t/3.9\ \mathrm{ns})}{23000\ \mu\mathrm{m}^3}. \qquad (13)$$

We use this approximation in the integral in the denominator of Eq. (12).

We obtain $N(t)$, the total number of orthoexcitons, by integrating the luminescence signal both over space and photon energy, then using our optical system calibration to convert the rate of luminescence counts to the number of orthoexcitons. Time-resolved spectra are recorded with 300-μm entrance and exit slits on the spectrometer, and the spectrally integrated signals are plotted in Fig. 17. During the initial 4 ns, the decay rate decreases with increasing time as expected for a density-dependent decay process. The solid curve is a fit to Eq. (12). N_0 was fixed at 3.5×10^9 which is the number of photons absorbed from the laser pulse times our measured 30% orthoexciton production efficiency. The other parameters were allowed to vary, resulting in the best-fit parameters:

$$t_0=(0.24\pm0.10)\mathrm{ns},$$

$$\tau=(3.24\pm0.10)\mathrm{ns},$$

$$\text{and } A=(6.6\pm1.0)\times10^{-17}\ \mathrm{cm}^3/\mathrm{ns}.$$

An alternative analysis to determine the Auger constant is to solve Eq. (9b) for A:

$$A=\frac{V(t)}{N(t)}\left(\frac{-1}{N(t)}\frac{dN(t)}{dt}-\frac{1}{\tau}+\frac{I(t)}{N(t)}\right). \qquad (14)$$

The approach is to use the experimental values of $N(t)$, $V(t)$, $I(t)$, and $dN(t)/dt$, and simply plot $A(t)$. The functional form for $I(t)$ is taken from a record of the laser profile, recorded in the same spectrometer with the same time-resolution as the luminescence. We normalize $I(t)$ to 3.5×10^9, determined from the laser pulse energy and our measured 30% orthoexciton production efficiency. Even after smoothing the data points, the derivative of $N(t)$ shows a lot of scatter, so we fit the data to a smooth function and use its derivative for $dN(t)/dt$. The fit is shown in Fig. 18(a). Figure 18(b) is a plot of Eq. (14) using this function. We see that in the region where the Auger decay rate is dominant, and the generation is mostly over, i.e., between 1 and 3 ns, A is quite stable and takes on the value of $(7.5\pm0.5)\times10^{-17}\ \mathrm{cm}^3/\mathrm{ns}$.

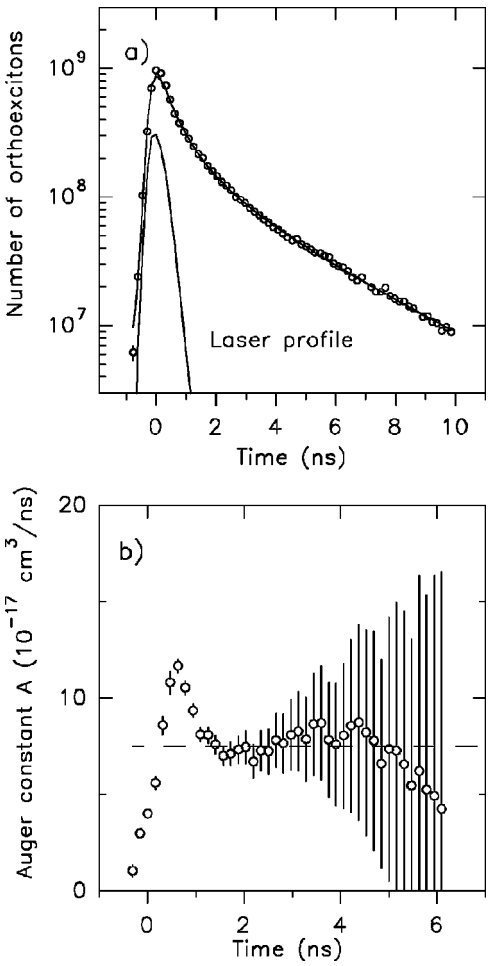

FIG. 18. (a) The same data as in Fig. 17, now shown with a smooth approximant for use in Eq. (14). The lower curve is the detected laser pulse shape. (b) The Auger constant A determined from Eq. 14 and the data in Figs. 16 and 17, plotted as a function of time. Error bars are one-σ uncertainties derived from uncertainties in the measured quantities entering into Eq. (14). At late times, uncertainty in $1/\tau$ dominates. To the extent that our model describes the physical system, this determination of A should be independent of time. The transient behavior before 1 ns may not be physically meaningful, due to the finite time resolution and its effect on our determination of $V(t)$.

VI. CONCLUSIONS

The values of the Auger constant derived from these two methods of analysis average to $7\times10^{-17}\mathrm{cm}^3/\mathrm{ns}$. Giving consideration to possible systematic errors and to the limits of our simple model, we trust this measurement to be within a factor of two of the Auger constant for orthoexciton-orthoexciton collisions defined by $dn_o/dt=-An_o^2$.

This Auger constant is two orders of magnitude larger than previous estimates.[26] The previous experiments either utilized continuous excitation without taking into account spatial diffusion[12] or they assumed densities given by spectroscopic fits to quantumlike energy distributions.[11] Our value agrees well with that determined by Trauernicht *et al.*[15] for paraexcitons confined to a strain well, an experiment in which both volume excitation was employed and spatial distribution of the gas was determined.

There is, however, other experimental evidence that orthoexcitons and paraexcitons display significantly different Auger decay rates: Lin and Wolfe[7] found that, while the orthoexciton signal followed the 10-ns laser pulse shape at early times, the decay of the paraexciton luminescence was considerably slower. If the orthoexcitons and paraexcitons in that experiment are occupying the same volume, then the Auger cross section for paraexcitons must be smaller. Kavoulakis and Baym[17] have pointed this out and present theoretical arguments that the Auger decay for paraexcitons should be considerably slower than that for orthoexcitons. While we cannot clearly see a fast decay of the paraexcitons in our present experiments (Fig. 5), we do see that the number of paraexcitons after the laser pulse increases nonlinearly with laser power. We conclude that paraexcitons are not immune to Auger losses.

The Auger rate can be characterized by a scattering cross section, σ_A, from the correspondence $1/\tau_A = n\sigma_A v = An$, giving $\sigma_A = A/v$. If we assume $v = 10^6$ cm/s for excitons at $T = 30$ K, we find $\sigma_A = 700\ \text{Å}^2 = 4\pi(7.5\ \text{Å})^2$. For comparison, the Bohr radius of an exciton in Cu_2O is approximately 7 Å.

We claim to measure an exciton decay rate that is dependent on the exciton density, i.e., $1/\tau = An$. There is, however, a secondary effect of Auger recombination that could further shorten the exciton lifetime. Some of the band-gap energy, which is released in each Auger recombination, appears as kinetic energy in the exciton gas.[11,12] The higher kinetic energy of the excitons could lead to a shorter lifetime through mechanisms other than collisions with other excitons. For example, one might consider ortho-para conversion to be the source of the rapid decay of orthoexcitons at early times. Snoke *et al.*[27] characterized this process as a *k*-dependent process, which would lead to a more rapid orthoexciton decay at early times when the kinetic energy distributions are broad. However, there is no evidence of a strong increase in the paraexciton population when the orthoexcitons exhibit a density-dependent decay, which would be a consequence of this process.

The unexpected strength of two-exciton Auger decay in Cu_2O puts severe limits on the densities attainable with pulsed laser excitation. This limitation of the gas density, coupled with the heating of the gas by the energy released in Auger recombination, makes prospects for Bose-Einstein condensation in Cu_2O seem unfavorable. However, orthoexciton kinetic energy distributions which are closely fit by saturated Bose-Einstein distributions, as one would expect at the critical density for condensation, have been seen many times.[2,6–12] The orthoexciton distributions created for this work also appeared to be nearly saturated Bose distributions with temperatures on the order of 30 K, but the maximum measured exciton density was $2\times10^{17}/\text{cm}^3$, which is near the critical density for condensation at 2 K.

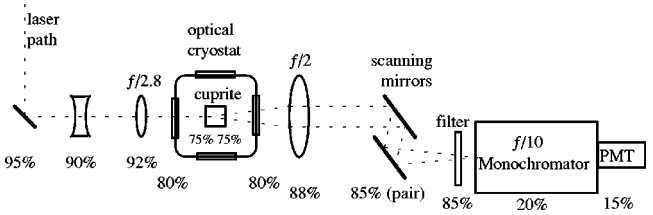

FIG. 19. Typical experimental arrangement, with transmission efficiencies of the various components (measured using 633 nm He-Ne laser light). The counting efficiency η defined in the text is the product of all the efficiencies to the right of the sample.

With the knowledge that the Auger recombination rate is as large as what one might expect for elastic scattering rates between excitons (see σ_A three paragraphs above) we hesitate to assume that the exciton gas is in quasiequilibrium with a well defined thermodynamic temperature. If the gas is not in quasiequilibrium, one should not interpret the kinetic-energy distribution as an equilibrium distribution at some effective gas temperature. We have turned instead to considering the exciton gas as a completely nonequilibrium system. Work is in progress to model the evolution of the exciton gas, accounting for phonon emission, Auger recombination and heating, ortho-para conversion, and spatial diffusion, in hopes of reconciling the suggestive spectral shapes with our measured densities.

ACKNOWLEDGMENT

This work was supported by the National Science Foundation under Grant No. NSF DMR 92-07458.

APPENDIX: COUNTING EXCITONS IN THE LAB

Our goal is to measure the exciton density, the number of excitons occupying a certain volume. The radiative rate derived in Sec. IV gives the photon flux produced by a given number of excitons. In this section we estimate the efficiency with which we count these photons, using the optical system diagrammed in Fig. 19.

The collection lens is a 90-mm fixed-focus $f/2.0$ camera lens. Focusing the luminescence on the monochromator entrance slit requires moving the lens further from the source than its design working distance. The most restrictive aperture is then the 28-mm-diameter aperture on the cryostat side of the lens, which is 70 mm from the luminescence, giving an effective aperture of $f/2.5$. The cone of light accepted by this lens has a half angle $\theta = \tan^{-1}(1/5)$. Snell's law reduces the cone of acceptance inside the crystal to $\theta' = \sin^{-1}[(1/n)\sin\theta]$. The solid angle, inside the cuprite, of the collected light is then

$$\Omega_{\text{collection}} = \int_0^{2\pi} d\phi \int_0^{\theta'} \sin\theta, d\theta$$

$$\approx \pi\theta'^2 \approx \pi\theta^2/n^2 \approx \pi/(5^2 n^2) = 0.014.$$

The efficiency of the monochromator is measured in conjunction with that of the photo-multiplier tube (PMT) and associated electronics. Typically, the combined efficiency is 1.8% for **E** vertical, 4.2% for **E** horizontal, using the monochromator in second order at 610 nm. The efficiency was checked at least every six months, since the PMT degrades with age and with use.

We assume that photons reflected from each optical surface are not re-reflected in such a way as to be counted. Combining the reflective losses with the monochromator and PMT efficiencies results in a counting efficiency η which is typically 1%. The conversion from number of orthoexcitons to PMT count rate is

$$\frac{\Omega_{\text{collection}}}{4\pi}\frac{\eta}{\tau_{\text{rad}}} \approx 0.8 \text{ counts per second per orthoexciton.}$$

The front slit of the monochromator (typically 100 μm wide) admits only a portion of the image of the exciton cloud. The magnification factor between the exciton cloud in the crystal to its image on the monochromator entrance was 5.4, so a typical 100-μm-wide entrance slit admits photons from a 19-μm-wide section in the sample. Of the photons that enter the monochromator, the rear slit allows only those with energy in a certain range to fall on the photocathode of the PMT. We have a monochromator with focal length $f=1$ m using a grating with line spacing $d=833$ nm in order $m=2$ and with an angle $2\phi=9.8°$ between incident and diffracted beams. A back slit width w will pass photons with wavelength in a range $\delta\lambda$ (wave number in a range $\delta\nu$) given by

$$\frac{\delta\lambda}{\lambda}=\frac{\delta\nu}{\nu}=\frac{1}{2}\frac{w}{f}\sqrt{\left(\frac{2d\cos\phi}{m\lambda}\right)^2-1}.$$

For the case of $h\nu=2024$ meV ($\lambda=612$ nm) and $w=100\ \mu m$, this formula predicts $\delta(h\nu)=0.09$ meV and we have measured $\delta(h\nu)=0.08$ meV.

When recording time-resolved luminescence, we accumulate photon counts resulting from $N_{\text{pulses}}\approx 10^6$ laser pulses; typically one photon is counted for every 10^3 laser pulses. Each counted photon increments one counter in an array of counters, based on the time between the laser pulse and the luminescence photon detection. To record a time-resolved spectrum, this process is repeated for the set of wavelengths we wish to sample. Thus each counter represents the number of luminescence photons counted within an energy range $\delta(h\nu)$, within a time range δt, accumulated over N_{pulses} repetitions of the experiment.

The results of a time-resolved luminescence experiment can be put into a canonical form by dividing the final value in each counter by N_{pulses}, by δt, and by $\delta(h\nu)$. The result is the number of *counts per second per meV per laser pulse* collected from the sample. The spectra in Figs. 2 and 3 have been treated in this way. The integral over the Γ_{12}^{-} phonon-assisted line in Fig. 3(a) at 0.3 ns is 0.9×10^8 counts per second, indicating that at this instant there were

$$0.9\times10^8 \text{cps} \div \left(\frac{\Omega_{\text{collection}}}{4\pi}\frac{\eta}{\tau_{\text{rad}}}\right) = 1.1\times10^8 \text{orthoexcitons}$$

in view of the spectrometer.

[1] J.B. Grun, M. Sieskind, and S. Nikitine, J. Phys. Chem. Solids **19**, 189 (1961).

[2] D. Hulin, A. Mysyrowicz, and C. Benoit à la Guillaume, Phys. Rev. Lett. **45**, 1970 (1980).

[3] We cool the liquid nitrogen to 69 K by pumping its vapor down to 250 torr, then repressurize the cryostat with helium gas. The liquid nitrogen will then evaporate, rather than boil, and remain below 71 K for the duration of the experiment.

[4] The theoretical energy distributions of hot carriers undergoing phonon relaxation and Auger decay is not a trivial problem and will be considered in a future paper.

[5] D.W. Snoke, D. Braun, and M. Cardona, Phys. Rev. B **44**, 2991 (1991).

[6] D.W. Snoke, J.P. Wolfe, and A. Mysyrowicz, Phys. Rev. Lett. **59**, 827 (1987); **64**, 2543 (1990); Phys. Rev. B **41**, 11 171 (1990).

[7] J.L. Lin and J.P. Wolfe, Phys. Rev. Lett. **71**, 1222 (1993).

[8] T. Goto, M.Y. Shen, S. Koyama, and T. Yokouchi, Phys. Rev. B **55**, 7609 (1997).

[9] N. Naka, S. Kono, M. Hasuo, and N. Nagasawa, Prog. Cryst. Growth Charact. Mater. **33**, 89 (1996).

[10] M.Y. Shen, T. Yokouchi, S. Koyama, and T. Goto, Phys. Rev. B **56**, 13 066 (1997).

[11] D.W. Snoke and J.P. Wolfe, Phys. Rev. B **42**, 7876 (1990).

[12] A. Mysyrowicz, D. Hulin, and C. Benoit à la Guillaume, J. Lumin. **24**, 629 (1981).

[13] G.M. Kavoulakis, G. Baym, and J.P. Wolfe, Phys. Rev. B **53**, 7227 (1996).

[14] D.P. Trauernicht and J.P. Wolfe, Phys. Rev. B **33**, 8506 (1986).

[15] D.P. Trauernicht, J.P. Wolfe, and A. Mysyrowicz, Phys. Rev. B **34**, 2561 (1986).

[16] Trauernicht *et al.* report an Auger constant $a=0.05$/s for paraexcitons confined to a Gaussian cloud by a strain well. This value must be multiplied by the appropriate volume—3×10^{-6} cm^3 using Eq. (10) later in this paper and the description of the strain well by Trauernicht *et al.*— and divided by 2 due to a difference in definitions.

[17] G.M. Kavoulakis and G. Baym, Phys. Rev. B **54**, 16 625 (1996).

[18] The density approaches steady state as $\exp(-\sqrt{AG}t)$, so to reach this steady-state value within a pulse of length T requires $\sqrt{AG}T \gg 1$.

[19] To the extent that the Auger cross section for ortho-para collisions may be larger than that for ortho-ortho collisions, Auger recombination would drive the paraexciton number lower, keeping the magnitude of the effect of paraexcitons the same.

[20] A. Mysyrowicz, D. Hulin, and A. Antonetti, Phys. Rev. Lett. **43**, 1123 (1979).

[21] F.I. Kreingol'd and V.L. Makarov, Fiz. Tverd. Tela (Leningrad) **17**, 472 (1975) [Sov. Phys. Solid State **17**, 297 (1975)].

[22] B. Karlsson, C.G. Ribbing, A. Roos, E. Valkonen, and T. Karlsson, Phys. Scr. **25**, 826 (1982).

[23] The actual situation in Cu_2O is somewhat more complicated. The optical transitions in question are phonon assisted, so we must consider the energies of the optical phonons created or de-

stroyed. We balance the *redshifted* absorption—seen in Fig. 5(b)—with the redshifted luminescence. Letting f_{12} denote the occupation number of the Γ_{12}^- optical phonon, the rate for this redshifted absorption is

$$(c/n)\alpha(\varepsilon)\rho(\hbar\omega)f_{12}f_p(1+f_x),$$

and the luminescence rate is

$$(1/\tau_{\rm rad})g(\varepsilon)(1+f_{12})f_x(1+f_p).$$

The energies of the photon and exciton are not equal; the total energy of the exciton is lower than that of the photon by one Γ_{12}^- phonon energy. Since in equilibrium all the f's are Planck functions, we have the following identity:

$$f_{12}(E_{12})f_p(\hbar\omega)[1+f_x(\hbar\omega+E_{12})]$$
$$=[1+f_{12}(E_{12})]f_x(\hbar\omega+E_{12})[1+f_p(\hbar\omega)].$$

So the final result is the same as Eq. (6) in the text.

[24] P.Y. Yu and Y.R. Shen, Phys. Rev. B **12**, 1377 (1975).
[25] P.D. Bloch and C. Schwab, Phys. Rev. Lett. **41**, 514 (1978).
[26] Reference 12 reported $A=2\times10^{-19}$ $\rm cm^3/ns$ and Ref. 11 reports a cross section which implies that $A\sim10^{-18}\rm cm^3/ns$ in order of magnitude.
[27] D.W. Snoke, D.P. Trauernicht, and J.P. Wolfe, Phys. Rev. B **41**, 5266 (1990).